HHS Public Access

Author manuscript

Nat Mater. Author manuscript; available in PMC 2016 May 18.

Published in final edited form as:

Nat Mater. 2015 December ; 14(12): 1269–1277. doi:10.1038/nmat4407.

Matrix Elasticity of Void-Forming Hydrogels Controls Transplanted Stem Cell-Mediated Bone Formation

Nathaniel Huebsch[1,2,3,*], **Evi Lippens**[1,2,4], **Kangwon Lee**[1,2], **Manav Mehta**[1,2,4], **Sandeep T Koshy**[1,2], **Max C Darnell**[1,2], **Rajiv Desai**[1,2], **Christopher M. Madl**[1], **Maria Xu**[1], **Xuanhe Zhao**[1,5], **Ovijit Chaudhuri**[1,2,7], **Catia Verbeke**[1,2], **Woo Seob Kim**[1,2,6], **Karen Alim**[1], **Akiko Mammoto**[8], **Donald E. Ingber**[1,2,8], **Georg N Duda**[4], and **David J. Mooney**[1,2]

[1]Harvard University School of Engineering and Applied Sciences, Universitätsmedizin Berlin and Berlin-Brandenburg Center for Regenerative Therapies, Berlin

[2]Wyss Institute for Biologically Inspired Engineering, Universitätsmedizin Berlin and Berlin-Brandenburg Center for Regenerative Therapies, Berlin

[3]Harvard-MIT Division of Health Sciences and Technology, Universitätsmedizin Berlin and Berlin-Brandenburg Center for Regenerative Therapies, Berlin

[4]Julius Wolff Institute, Charité – Universitätsmedizin Berlin and Berlin-Brandenburg Center for Regenerative Therapies, Berlin

[5]Duke University Department of Mechanical Engineering, Chung-Ang University, Heuk Seok-Dong, Dong Jak-Gu, Seoul, Korea

[6]Department of Plastic Surgery, College of Medicine, Chung-Ang University, Heuk Seok-Dong, Dong Jak-Gu, Seoul, Korea

[7]Stanford University Department of Mechanical Engineering, Children's Hospital and Harvard Medical School

[8]Vascular Biology Program, Departments of Pathology & Surgery, Children's Hospital and Harvard Medical School

Abstract

The effectiveness of stem-cell therapies has been hampered by cell death and limited control over fate[1]. These problems can be partially circumvented by using macroporous biomaterials that improve the survival of transplanted stem cells and provide molecular cues to direct cell phenotype[2–4]. Stem cell behavior can also be controlled *in vitro* by manipulating the elasticity of both porous and non-porous materials[5–7], yet translation to therapeutic processes *in vivo* remains elusive. Here, by developing injectable, void-forming hydrogels that decouple pore formation from elasticity, we show that mesenchymal stem cell (MSC) osteogenesis *in vitro*, and cell deployment

*Current affiliation: Gladstone Institute of Cardiovascular Disease, San Francisco, CA 94158

Author Contributions The experiments were designed by NH, EL and DJM and carried out by NH, KL, MM, AM, MCD, RD, STK, CV, EL, CMM, MX, OC, WSK, and XZ. MM, GD, KA, MB, AM, and DEE provided new reagents and analytical tools. The manuscript was written by NH and DJM. The principal investigator is DJM.

in vitro and *in vivo*, can be controlled by modifying, respectively, the hydrogel's elastic modulus or its chemistry. When the hydrogels were used to transplant MSCs, the hydrogel's elasticity regulated bone regeneration, with optimal bone formation at 60 kPa. Our findings show that biophysical cues can be harnessed to direct therapeutic stem-cell behaviors *in situ.*

Keywords

Cell Delivery; Cell Therapy; Porogen; Mechanotransduction

Endogenous stem cell niches provide an optimal micro-environment for stem cell maintenance, and also facilitate stem cell deployment in response to host injury[4,8]. One particular niche component, the extracellular matrix (ECM), has been identified as a particularly important source of cues that direct cell fate decisions. Biomaterials have been designed to mimic these niches by presenting specific signaling cues to modulate stem cell expansion, migration and gene expression[2–4,9]. Biophysical aspects of the ECM, including elasticity, have been linked to a variety of cellular behaviors *in vitro* and *in vivo* using hydrogel systems[5,6,10]. However, current materials used to manipulate cell fate via matrix elasticity (e.g. mechanotransduction) in 3D limit cell motility, proliferation or new tissue formation[6,11]. Materials used to elicit tissue formation via transplanted cells must also degrade to allow space for new tissue formation[12,13]. Unlike materials used to study mechanobiology *in vitro*, these transplantable, degradable scaffolds typically exhibit mechanical properties that change continuously over time, making it difficult to study relationships between matrix mechanics and cell behavior. Slowly degrading macroporous sponges fabricated from polymers such as poly(lactide-co-glycolide) exhibit a structure compatible with tissue ingrowth[14], but these protein-fouling materials do not allow precise control of the cell-material interface, making it difficult to control transplanted cell behavior through defined insoluble cues.

To address the limitations of current materials, we developed void-forming hydrogels. Within these materials, cells are initially encapsulated into a nanoporous hydrogel milieu that subsequently form pores *in situ*, after injection into host tissues. Current techniques used to create macroporous biomaterials rely on extraction of porogen templates by solvents[7,15,16], *in situ* degradation of soft materials[17], phase inversion [18], cell-mediated degradation of single phase hydrogels[19], or 3D printing[20]. A significant drawback of scaffold-based methods is that they typically do not allow simple delivery of the material via injection. While enzymatically degradable, single-phase hydrogel materials offer elegant control over cellular invasion, cell confinement within these systems remains strongly coupled to matrix elasticity, and enzyme-mediated changes to local mechanical properties may be difficult to control in a pre-determined manner. Exogenous mechanical stimulation of cells in 3D culture alters their Matrix Metalloproteinase (MMP) activity[21], suggesting it is likely that mechanotransduction pathways triggered by the interaction of cellular contractile forces and matrix elasticity will also alter MMP activity in these hydrogel systems. In turn, this may make it difficult to decouple matrix elasticity from micron-scale cellular protrusion into the material.

We hypothesized that the aforementioned drawbacks could be overcome with a system wherein solid-phase porogens could be first encapsulated into a bulk hydrogel, but then degrade via hydrolysis, resulting in the creation of voids within the hydrogels after placement in physiologic conditions (fig. 1a). Importantly, the rate of pore formation and subsequent cell release, endogenous cell infiltration and tissue formation would then be controlled by the rate of porogen degradation and cell migration and proliferation within pores. This would decouple the elasticity of the slowly degrading, "bulk" component (fig. 1a, grey) from cell confinement by the gel, with the rate of void-formation and cell release pre-determined via the chemical composition of porogens. Furthermore, these composite materials could be introduced into the body in a minimally invasive manner as long as the porogens within were smaller than the diameter of the injection needle.

To test the possibility of fabricating void-forming hydrogels, mechanically rigid, but rapidly degrading sacrificial gel porogens of an appropriate size (~150μm diameter; fig. S1) were formed from oxidized, hydrolytically labile alginate[22], and encapsulated into a "bulk" hydrogel comprised of slowly degrading, high molecular weight alginate (fig 1b,S1). To assess the possibility of void formation *in situ*, we first performed scanning electron microscopy on composite gels that were flash-frozen in liquid nitrogen at different time-points after formation. These studies suggested time-dependent void-formation (fig. S2), but because of concerns about artifactual pore formation during freezing and lyophilization, we developed a fluorescence assay to directly analyze void-formation within intact hydrogels (fig. 1b). Simultaneous *in situ* fluorescence analysis of the porogens (green) and bulk component (red) of void-forming hydrogels revealed that porogens were initially intact, but degraded *in-situ* to form voids (fig. 1b). Quantifying the kinetics of porogen degradation revealed a time-scale of approximately one week for the majority of porogen degradation (fig. 1c,d). Consistent with these studies, rheological analysis of the shear modulus G' of these composite materials seven days after formation indicated a porogen-density dependent decrease in G' in void-forming hydrogels, as compared to intact, standard hydrogels (not containing porogen) at day 0 (fig. 1e). When the density of pores was above 50%, the relationship between pore concentration and the decrease of G' was nearly linear (fig. 1e), consistent with theoretical predictions of the mechanical behavior of pore-filled solids[23].

The effects of pore formation on encapsulated cell morphology and distribution within the void-forming hydrogels were next analyzed. Clonally derived mouse mesenchymal stem cells (mMSC; D1, ref. [24]) were used as a cell model. Previous studies involving non-porous hydrogels indicate these cells and human MSC exhibit similar responses to matrix composition, but that D1 demonstrate less spontaneous osteogenic differentiation than primary human MSC[6,25]. The bulk phase of hydrogels was modified with peptides which present the integrin binding RGD motif, to provide a defined mechanism for cell adhesion[26], and the density of porogens was held constant at 50% of the total volume of void-forming hydrogels. The overall morphology of mMSC was initially similar in standard and void-forming hydrogels. In contrast, after void formation, cells adjacent to pores exhibited extended distended, spread morphology (fig. 1f), whereas cells in standard hydrogels, or those that were far from the pore phase within void-forming hydrogels, maintained a rounded morphology consistent with past reports[6,27]. Apparent changes in cell morphology were verified with phalloidin staining (fig. 1g). Over longer time-frames, pore formation led

to enhanced cellularity and the presence of large cell clusters spanning significant distances within the composite material (fig. 1f). This increase in apparent cellularity, although partly caused by morphology changes, was also due to cell proliferation. Proliferation could be controlled based on the dose of RGD presented by the bulk component of void forming hydrogels (fig. 1h-j). As cell encapsulation into alginate hydrogels is highly efficient and does not depend on RGD density (data not shown), these results indeed reflect the influence of RGD on cell proliferation (rather than initial cell density).

Given the ability to form void-forming hydrogels, and the interest in applying these materials to test the ability to use matrix elasticity to control transplanted cell behavior, we next performed *in vitro* studies to determine the effects on MSCs of modulating the elasticity of the RGD-modified bulk phase. At a fixed density of RGD peptides (375μM) previously established to induce osteogenesis of hMSC in 3D culture[6], and a porogen volume density of 50%, mMSC proliferation and osteogenic commitment were analyzed (fig. 2). Cell proliferation exhibited a biphasic dependence on matrix elasticity, peaking within materials of intermediate stiffness (fig. 2a). Osteogenic lineage commitment, assessed via Alkaline Phosphatase (ALP) activity in deployed cells, was also optimal with intermediate bulk matrix elasticity (fig. 2b). These findings are consistent with previous work which indicated high levels of integrin occupancy occurred in 3D materials with intermediate elastic modulus[6]. Consistent with previous literature linking cell-matrix mechanics to differentiation of pre-osteoblasts[28], we observed a marked effect of matrix elasticity on Mitogen Activated Protein Kinase (MAPK) signaling, as assessed by MAPK Thr202/Tyr204 phosphorylation within cells remaining in void-forming hydrogels after seven days of culture (fig. 2c,d). To further verify the effect of bulk component elasticity on osteogenic behavior of encapsulated MSC, more definitive markers of osteogenesis were assessed. Collagen I expression and mineralization by mMSC both occurred within void-forming hydrogels in an elasticity-dependent manner (fig. 2e-g). These results are consistent with previous studies involving non-porous, RGD-modified cell encapsulating hydrogels, which indicated a biphasic effect of E on osteogenesis[6], in materials that prevented cell migration and also limited proliferation. Normalizing collagen I expression to cell number did reveal a subtle effect of proliferation on total osteogenesis (fig. 2h) – however, the biphasic relationship between matrix elasticity and osteogenic marker expression was preserved.

As the elasticity of the cell-interactive phase of void-forming hydrogels could be tuned to modulate MSC osteogenesis, we next investigated the application of these materials for cell deployment *in vitro*, to test their potential ability to support transplanted cell deployment and ingrowth of newly formed endogenous tissue. As cell deployment was expected to occur via channels of interconnected voids spanning from the surface through the interior of the material, initial studies were performed to determine the minimum density of porogens required (Supplemental Materials). For infinitely large composite gels, a percolating network of porogens would be required, and this would lead to a minimum porogen volume fraction near 65%. However, given the ultimate size of gels used in these studies (2mm diameter for *in vitro* studies, with injection volumes of 100μL for *in vivo* studies), and the size of porogens (~150μm diameter), numerical simulations predicted effective percolation of voids (e.g. high likelihood of voids spanning through the material) with porogen fraction of 50%. Although a volume fraction of 50% porogens was not sufficient for interconnected

void-formation as assessed by a capillary assay (Supplemental Materials, fig. S3), it was more than sufficient to allow cell release. Because this lower porogen volume fraction (50%) facilitated specimen handling, particularly with void-forming gels with a soft bulk component, this porogen density was used in all subsequent analyses.

The dependence of cell deployment kinetics on porogen material properties was next investigated. Cell deployment was monitored by measuring alamar blue reduction by cells that had deployed out of gels, onto the underlying plastic substrate, after verifying that this methodology produced similar estimates of cell release as direct, manual counts (fig. S3b). Pore formation led to substantial cell deployment from void-forming hydrogels, whereas little release occurred from standard gels with the same composition as the bulk component of void-forming hydrogels (fig. 3a). The total number of cells deployed exceeded the number of cells initially encapsulated in the void-forming hydrogels, consistent with our previous observation of cell proliferation within these materials (fig. 1h-j). Importantly, the kinetics of deployment and overall number of released cells could also be controlled by manipulating two porogen fabrication parameters: the concentration of hydrolytically labile groups in the polymers used to form porogens, and the concentration of divalent cation used to crosslink porogens (fig. 3b,c). At a constant porogen density and RGD density (375μM, the same density used for *in vitro* osteogenesis assays), increasing the bulk gel elasticity diminished cell deployment (fig. 3d). Diminished cell release from materials with higher elastic moduli may reflect a higher adhesivity that prevents cell detachment[29], or an inability of the cells to deform the gels sufficiently to enable their migration through the material to access the pores[7]. Interestingly, net cell deployment from void-forming hydrogels with constant bulk component elasticity (60 kPa) was not affected by RGD density (fig. 3e). This is in contrast to previous work linking cell-ECM adhesiveness to cell migration speed[29]. The apparent discrepancy between these results may result from changes in cell migration speed being matched by changes in cell proliferation, which substantially increased as the density of RGD peptides was raised from 0 to 750μM. Based on this finding, it is most likely that modulating bulk matrix elasticity affected cell release by altering cells' ability to mechanically deform the hydrogel surrounding voids, as they migrate through the composite material.

Cell deployment from void-forming hydrogels *in vivo* was analyzed using genetically labeled cells within hydrogels transplanted subcutaneously in nude mice. In the first week following cell transplantation, there was a slight (30%) decrease in the fluorescent signal from the mCherry-labeled mMSC for all transplantation conditions. Following this slight decrease, mMSC delivered within standard, nanoporous hydrogels were released to a modest extent, but only after several weeks (fig. 3f,g; S4), achieving a final density about 9.5-fold as high as at day 7. However, mMSC delivered within void-forming hydrogels were released much more rapidly and proliferated markedly, over the same time-scale on which pores formed, finally achieving a 31-fold increase over the density at day 7. Consistent with *in vitro* studies, both the overall number of mMSC and the kinetics of their deployment from pore-forming gels could be controlled by modulating porogen characteristics (fig. 3g). Further, the number of deployed cells increased substantially when the density of peptides in the bulk gel was increased (fig. 3h). Finally, within a cranial defect model, the generation of voids spanning the material and concomitant mMSC release could be detected histologically

within one week of cell encapsulation within void-forming hydrogels (fig. 3i). Cells released from these void-forming hydrogels were found at distances up to 350μm away from the gels. In contrast, mMSC were retained in standard hydrogels (fig. 3j).

As void-forming hydrogels could control MSC deployment, differentiation and proliferation *in vitro*, as well as expansion and dissemination of cells *in vivo*, we next investigated whether these materials could be used to enhance the effects of transplanted MSC on bone regeneration. Human MSC (hMSC), either in saline, standard hydrogels, or void-forming hydrogels were directly injected into freshly formed critically-sized cranial defects in nude rats. Both standard and void-forming hydrogels had constant bulk composition (150μM RGD, 60 kPa), which was chosen to match the properties of hydrogels previously demonstrated to elicit ectopic bone formation *in vivo* by encapsulated osteoblasts and chondrocytes[30]. Bone growth was evaluated 12 weeks after cell transplantation. Paralleling results from clinical studies involving direct stem cell transplantation[1], bolus delivery of hMSC alone in the nude rat model had only modest effects on bone regeneration, as measured by micro-computed tomography (fig. 4a,b).

Transplantation of hMSC within standard, nanoporous hydrogels improved bone regeneration compared to the bolus injection group (fig. 4b, S5). hMSC transplantation within void-forming hydrogels led to a further, statistically significant increase in the amount of new bone formation, compared to cells alone (fig. 4a,b). Histologic analysis revealed that when hMSC were delivered via saline bolus, much of the newly formed bone was near the margin of the original defect, likely reflecting ingrowth of tissue adjacent the defect, rather than new bone formation (fig. S5). Delivery with nanoporous gels led to large masses of hydrogel remaining in the defect site, and the osteogenic tissue that had formed in this condition was often contained within the remaining hydrogel and not in continuity with host tissues (fig. S5).

Compared to standard hydrogels, void-forming gels left a much smaller amount of remaining gel material 12 weeks following transplantation (fig. S5), and analysis of trichrome stained sections also revealed the presence of osteoblasts emanating from the small fragments of residual material in void-forming gels near the center of defects, consistent with the assumption that cells that directly interact with the material contributed to new bone formation (fig. S5). To determine the origin of the newly generated bone, we performed fluorescence *in situ* hybridization (FISH) studies to detect the primate specific Alu repeat mRNA sequence, on samples obtained after 4 weeks. Although mineralization had already occurred at this time point, it was less extensive than at 12 weeks, making FISH analysis feasible. At four weeks, although there were clearly detectable human cells remaining within both standard and void-forming hydrogels, the vast majority of cells were non-primate (rodent) in origin (fig. S5). These results suggest that transplanted cells either served as a source of osteogenic cytokines, or recruited endogenous rodent cells, which subsequently interacted with the gel to form bone. This hypothesis may be testable via implantation of acellular hydrogels, either with or without cytokine loading. However, precisely matching cell-mediated cytokine delivery in terms of specific proteins and kinetics may prove challenging[31].

Finally, studies were performed to test the hypothesis that matrix elasticity regulates bone formation by transplanted stem cells. Strikingly, new bone formation exhibited a marked dependence on bulk matrix elasticity, with optimal regeneration occurring within materials with an intermediate elastic modulus (60 kPa; fig. 4c-f). The volume of new bone generated with void-forming gels that did not exhibit this optimal elastic modulus was not statistically different compared to bone generated by transplanting cells in saline (fig. 4a).

The effect of matrix elasticity on bone regeneration was found at 12 weeks, although the modulus of the material would be expected to diminish slightly by this time. This finding is consistent with previous data suggesting that MSC commit during their first 1–2 weeks in a mechanically optimal micro-environment, even if the mechanical cues vary after that time[5,6]. Moreover, MSC-derived cells that were cultured under these osteo-permissive 3D conditions *in vitro* were previously shown to elaborate osteogenic cytokines such as osteocalcin[6], and this may have contributed to fate decisions within transplanted hMSC and stimulation of bone formation by endogenous cells. μCT analysis of the bone mineral density and trichrome staining of tissue sections also suggested that the quality of newly formed bone was greatest at the intermediate bulk gel stiffness (fig. 4e-g). Finally, trichrome staining of sections derived from defects into which hMSC were delivered from hydrogels of optimal elasticity revealed newly formed bone with entrapped cells and osteoblasts on the bone surfaces, suggesting that tissue formation within the defect site mimics hallmarks of endogenous bone formation (fig. 4h-j).

The elastic modulus found in these studies to best induce bone formation and stimulate defect repair is similar to the optimal range found to induce osteogenic gene and protein expression in encapsulated MSC in nanoporous gels *in vitro*[6]. This suggests that mechanotransduction pathways that regulate stem cell gene and protein expression *in vitro* might be directly transferred to complex *in vivo* processes such as bone formation. Because the pore size of hydrogels used in that previous work were not permissive to cell migration or marked expansion, this result further suggests that at least part of the contribution of matrix elasticity to new bone formation is directly related to mechanically-induced osteogenesis, and not simply secondary to cells' ability to egress from gels. Furthering this notion that migration was not the sole determinant of mechanically-controlled bone formation in the present study was our *in vitro* observation that MSC deployment was most pronounced in void-forming gels with a bulk component elasticity near 5 kPa – a range that was not compatible with new bone growth. Nevertheless, the bone repair we observed likely required some cell migration and proliferation and the ability of hydrogels with elasticity in the 60 kPa range to support these processes (based on *in vitro* assays, fig. 2a,b, 3d) was also likely important for transplanted cell-mediated tissue repair.

Previous *in vitro* work has demonstrated that with hydrogels that exhibit a high degree of swelling, changes in nanometer-scale ligand distribution resulting from changes in substrate crosslinking may have a more pronounced effect on MSC behavior than do corresponding changes in matrix elasticity[32]. However, the results of the current study and other work with similar hydrogels that exhibit more limited changes in swelling, ligand density and nanometer-scale adhesion ligand distribution as elastic modulus is altered demonstrate direct effects of E on stem cell behavior[6,33,34]. Recently developed materials in which secondary

crosslinks can be formed *in situ*, or in which crosslinks can be degraded *in situ*, in the presence of cells, offer an elegant experimental approach to study temporal requirements for matrix elasticity to control cellular mechanotransduction *in vitro*[11, 35, 36]; however, causing void-formation on the size-scales required for cellular deployment out of, and infiltration into these types of gels *in vivo* would require novel methodologies for precisely delivering light into tissues.

Here, we demonstrate that mechanotransduction, previously shown to regulate mesenchymal stem cell fate *in vitro*[5, 6], and implicated in craniofacial development[37], can be harnessed to locally control stem cell mediated tissue repair *in situ*. Given the strong evidence that mechanotransduction pathways regulate a variety of other stem cell populations *in vitro*[33, 38], we anticipate that these biophysical cues might be useful in regenerating other tissues. The optimal stiffness found to induce new bone growth in the present studies is slightly higher than that reported for *in vitro* osteogenesis in nanoporous 3D gels. However, MSCs near a newly formed pore likely experience a slightly diminished modulus compared to the stiffness sensed in nanoporous hydrogels[39], and this may underlie the small discrepancy. The finding that bone regeneration was initiated in the absence of exogenous growth factors suggests that these mechanotransduction pathways act synergistically with low basal endogenous levels of osteogenic cytokines[37, 40]. Importantly, this suggests that optimally designed materials could be used to obtain highly localized control over transplanted cell fate, preventing deleterious off-target effects that have previously been observed when high levels of locally administered osteogenic cytokines can diffuse out of the intended application area[41].

Given the promise of harnessing mechanotransduction toward transplanted-cell mediated tissue repair, it will be important in future studies to define early changes in signaling and transcription networks that underlie later, functional changes in cell fate. In the present work, we identified a strong correlation between MAPK signaling and *in vitro* osteogenesis. However, the exact optimum for MAPK signaling (20 kPa) at day 7 differs from the optimum we observed for ALP activity and per-cell Collagen I expression (60 kPa) at day 14. This suggests the potential need to glean quantitative information on multiple signaling pathways, over multiple time-points to predict matrix-guided MSC fate[42]. Likewise, precise identification of the timing of activation of osteogenic transcription factors (e.g. Runx2, Osterix) would allow one to thoroughly explore the large variable space (elasticity, adhesion ligand density, rate of void formation, etc.) and identify optimal design parameters that induce the most efficient cell-mediated tissue repair.

We anticipate that void-forming hydrogels will provide a useful platform for future basic studies on cell-matrix interactions and translational studies involving cell therapies. Both the bulk hydrogel and porogen phases of these materials could be utilized in future work to deliver soluble cues to enhance regeneration. These materials could also be used to deliver inhibitory molecules (e.g. function blocking antibodies) in order to probe the molecular mechanisms through which cell-material interactions, or cellular interactions with host tissues, modify the fate of transplanted and endogenous cells[43]. Although not explored in the present work, the effects of biomaterial pore size on tissue formation and cell migration has been studied extensively in the past[7], and altering porogen size may facilitate enhanced

control over endogenous cell recruitment in future studies. Furthermore, if the degradation properties of the bulk material are modified to yield more permanent structures (for example, by incorporating covalent rather than ionic crosslinking), these injectable materials may be useful towards preserving the survival and phenotype of human cells transplanted in the context of humanized models of *in vivo* stem cell niches (e.g. bone marrow; ref. [44]). In contrast to materials that require surgical implantation or that mediate significant protein adsorption (e.g., poly(lactide-co-glycolide)), hydrogel materials used to fabricate void-forming gels may be less likely to induce inflammation or other processes that might interfere with the biology being analyzed. By uncoupling several biophysical cues shown to regulate cell fate *in vitro* – including porosity, matrix elasticity and matrix adhesivity[7], the strategy used to fabricate void-forming hydrogels allows these variables to be independently tuned to control cell fate. The ability to harness these cues *in situ* will likely be useful for cell-based therapies, as well as basic studies on the biology of cell-matrix interactions *in vivo*.

Methods Summary

Void-Forming Hydrogels

To form the rapidly degrading porogen phase, high M_w, high guluronic acid (GA)-content alginates (MVG; FMC biopolymer) were modified by oxidation of between 3–7.5% of GA residues with sodium periodate (Sigma; ref. [21]). Following dialysis, sterile filtration and lyophilization, binary mixtures of oxidized MVG combined with high M_w, unmodified MVG were dissolved into serum free Dulbecco's Modified Eagle Media (DMEM; Invitrogen). Polymer solutions were formed into gel beads by extruding through a glass atomizer with co-axial nitrogen air flow at a constant pressure (30 mmHg) into a bath of 25–100mM calcium chloride in 50–100mM HEPES buffer (pH 7.4) with constant stirring. After 5 minutes of crosslinking, gel beads were retrieved, and washed to deplete excess calcium. In some cases, alginate polymers used to form porogens were labeled with aminofluorescein (Sigma; ref. [45]) to facilitate analysis of porogen size and shape.

To form the slowly degrading, cell-interactive bulk gel phase, MVG alginates were covalently coupled with the integrin binding peptide $(Gly)_4$-Arg-Gly-Asp-Ala-Ser-Ser-Lys-Tyr (Peptides International; ref. [26]). In studies involving the effects of bulk gel elastic modulus on cells, RGD-modified MVG was combined with unmodified MVG or MVG that had been irradiated to reduce M_w but maintain crosslinking ability (ref. [46]). Void-forming hydrogels were formed by encapsulating cells and porogens into the bulk gel phase, and then crosslinking the bulk-gel phase with calcium sulfate. In some experiments, MVG used to form the bulk gel was labeled with tetramethylrhodamine cadaverine (Anaspec).

In vitro Osteogenesis Assays

Clonally derived derived mouse mesenchymal stem cells (D1; ref. [24], American Type Cell Culture, used at passages 20–24) were encapsulated into the bulk gel phase (20 million cells/mL of bulk gel, to mimic the density that would eventually be used for cranial defect studies) by mixing with polymer before addition of porogen beads and crosslinking. Immediately after crosslinking, composite hydrogels were transferred to tissue culture

polystyrene substrates with DMEM containing 10% Fetal Bovine Serum and 1% Penicillin/Streptomycin. To facilitate osteogenesis, 50μg/mL *L*-ascrobic acid and 10mM β-glycerol phosphate were also added to the media, which was exchanged every two days. At 7 and 14 days, hydrogels were transferred aseptically to fresh media in a fresh tissue culture plate. Care was taken to avoid damaging hydrogels during transfer. After moving gels on day 14, wells in the used plate were washed with PBS and then adherent cells were lysed into a passive lysis buffer (Promega). The nuclear and cytosolic fractions were next separated by centrifugation (14,000g, 20 minutes). DNA was liberated from the nuclear pellet (CyQuant lysis buffer, Invitrogen), and quantitated with Hoescht 33342, based on a standard curve generated with calf thymus DNA. Alkaline phosphatase (ALP) activity of the cytosolic fraction was quantitated with 4-MUP reagent (Sigma), with a standard curve provided by Calf Intestine Alkaline Phosphatase (Sigma). In parallel with these studies, void-forming gels containing cells were fixed at day 14, first in paraformaldehyde (to fix cells) and then in barium chloride, to fix hydrogels. Samples were then embedded into Optimal Cutting Temperature media (OCT) and flash frozen in liqud N_2. 10μm cryosections were then taken, which were stained with antibodies against Collagen I (ab34710, Abcam), with Hoescht 33342 for nuclear counterstaining. Mineralization was assessed in 25μm sections using Von Kossa staining. For immunoblot analysis of osteogenesis-related signaling in cells, day 7 void-forming hydrogels were removed from culture and washed with PBS. Next, cells were retrieved from hydrogels via calcium chelation with ice-cold 500mM EDTA. Cell pellets were washed in the same 500mM EDTA solution, and the pellets were flash-frozen in liquid nitrogen. Cells were lysed directly into SDS sample buffer, and 50 μg of protein were resolved by SDS-PAGE, transferred to a nitrocellulose membrane and then probed with antibodies against phospho-MAPK Thr202/Tyr204 (Cell Signaling, #9101) or total MAPK (Cell Signaling, #4696). GAPDH (Millipore, #Mab374) was used as a loading control.

In vitro Cell Deployment and Proliferation Studies

D1 mesenchymal stem cells (passages 20–24) were encapsulated into the bulk gel phase (2 million cells/mL of bulk gel) by mixing with polymer before addition of porogen beads and crosslinking. Immediately after crosslinking, composite hydrogels were transferred to tissue culture polystyrene substrates with DMEM containing 10% Fetal Bovine Serum and 1% Penicillin/Streptomycin. Every 3–7 days, hydrogels were transferred aeseptically to fresh media in a fresh tissue culture plate. Care was taken to avoid damaging hydrogels during transfer. Wells in the used plate were washed with PBS and then deployed cells that had adhered to the substrate were quantified via alamar blue assay (Invitrogen). A standard curve formed by plating serial dilutions of D1 cells was used to convert alamar blue reduction rates into cell numbers. The validity of this approach was tested at early time-points through direct comparison of cell counts obtained by alamar blue to cell counts obtained by trypsinizing cells and counting with a hemocytometer (fig. S3).

In vivo Cell Deployment Studies

All animal studies were performed under protocols approved by institutional guidelines (Harvard University Institutional Animal Care and Use Committee). D1 cells were transduced using pOC-mCherry retrovirus[10]. Cells were then encapsulated into the bulk phase of void-forming hydrogels, and composite gels were injected (2×10^6 cells per 100μL

injection) into the subcutaneous space in the flank of Nu/J mice (Jackson) via 18-gauge needles. Each mouse received two bilateral injections. Over the time-course of the study, the overall level of mCherry fluorescence, proportional to cell density, was measured using a Caliper Life Sciences IVIS Xenogen imaging system. Animals were anesthetized with isofluorane during imaging procedures. All animal experiments were performed according to established animal protocols. For studies of cell deployment within cranial defects, 8-mm critical-sized cranial defects were formed in Nude Rats (Charles River), and a constant volume of hydrogel (100μL) containing 2 million mCherry-expressing D1 was injected directly into the freshly formed defect. One week after transplantation, animals were euthanized, mineralized bone was decalcified (EDTA), and histologic sections were acquired which encompassed the defect area. Transplanted D1 were identified by immunohistochemical staining for mCherry (AbCam, 10μG/mL) visualized by DAB chromogen (Thermoscientific) on a background of tissue stained with hematoxylin.

Cranial Defect Studies

Human MSC (Lonza) were propagated in low glucose DMEM with 20% FBS and 1% Penicillin/Streptomycin to passage 2–6. Subsequently, cells were encapsulated into the bulk phase of void-forming hydrogels or standard hydrogels, or mixed into saline. Cranial defects were formed as described above, and a constant volume of hydrogel or saline (100μL) containing 2 million hMSC was delivered into the freshly formed defects. After the surgeries, animals were encoded so that microcomputed tomography (μCT) and histology could be performed in a blinded fashion. Animals were euthanized after 12 weeks, and bone regeneration was detected using (μCT) on a Viva40 micro-CT (Scanco Medical , AG®), at a voltage of 55 kV and current of 145 μA, integration time of 314 ms. Voxel size was selected to be isotropic and fixed at 35.5 μm. The scan axis was adjusted to be normal to the subject frontal plane. An established protocol for quantitative analysis of μCT scans was used to obtain measurements of bone volume and average mineral density of newly formed mineral within defects (ref. [47]).

Supplementary Material

Refer to Web version on PubMed Central for supplementary material.

Acknowledgements

We thank Suvai Gunasekaran for assistance with sample cryosectioning, Ruth Choa for assistance with histologic analyses, and Michael Brenner and Vinothan Manoharan (Harvard University) for discussions on percolation. We thank Kiichiro Tomodo, Po-Lin So and Edward Hsiao (Gladstone Institute, San Francisco) for helpful discussions and editorial suggestions. We also acknowledge support from the Materials Research Science and Engineering Center (MRSEC) at Harvard University (DM, XZ, NH), funding from NIH (R37 DE013033), the Belgian American Educational Foundation (EL), an NSF Graduate Research Fellowship (NH), an Einstein Visiting Fellowship (DM) and funding of the Einstein Foundation Berlin through the Charité – Universitätsmedizin Berlin, Berlin-Brandenburg School for Regenerative Therapies GSC 203, the Harvard College Research Program (CMM, MX) and Harvard College PRISE, Herchel-Smith and Pechet Family Fund Fellowships (MX).

References

1. Wollert KC, Drexler H. Cell therapy for the treatment of coronary heart disease: a critical appraisal. Nat Rev. Cardiol. 2010; 7(4):204–215. [PubMed: 20177405]

2. Silva EA, Kim ES, Kong HJ, Mooney DJ. Material-based deployment enhances efficacy of endothelial progenitor cells. Proc. Natl. Acad. Sci. USA. 2008; 105(38):14347–14352. [PubMed: 18794520]

3. Huebsch N, Mooney DJ. Inspiration and application in the evolution of biomaterials. Nature. 2009; 462(7272):426–432. [PubMed: 19940912]

4. Lutolf MP, Gilbert PM, Blau HM. Designing materials to direct stem-cell fate. Nature. 2009; 462(7272):433–441. [PubMed: 19940913]

5. Engler AJ, Sen S, Sweeny HL, Discher DE. Matrix Elasticity Directs Stem Cell Lineage Specification. Cell. 2006; 126:677–689. [PubMed: 16923388]

6. Huebsch N, et al. Harnessing traction-mediated manipulation of the cell/matrix interface to control stem-cell fate. Nat Mater. 2010; 9(6):518–526. [PubMed: 20418863]

7. Peyton SR, et al. Marrow-derived stem cell motility in 3D synthetic scaffold is governed by geometry along with adhesivity and stiffness. Biotechnol. Bioeng. 2011; 108(5):1181–1193. [PubMed: 21449030]

8. Scadden DT. The stem-cell niche as an entity of action. Nature. 2009; 441(7097):1075–1079. [PubMed: 16810242]

9. Yang F, Williams CG, Wang DA, Lee H, Manson PN, Elisseeff J. The effect of incorporating RGD adhesive peptide in polyethylene glycol diacrylate hydrogel on osteogenesis of bone marrow stromal cells. Biomaterials. 2005; 26(30):5991–5998. [PubMed: 15878198]

10. Mammoto A, et al. A mechanosensitive transcriptional mechanism that controls angiogenesis. Nature. 2009; 457:1103-U57. [PubMed: 19242469]

11. Khetan S, Burdick JA. Patternign network structure to spatially control cellular remodeling and stem cell fate within 3-dimensional hydrogels. Biomaterials. 2010; 31:8228–8234. [PubMed: 20674004]

12. Hutmacher DW. Scaffolds in tissue engineering bone and cartilage. Biomaterials. 2000; 21(24): 2529–2543. [PubMed: 11071603]

13. Simmons CA, Alsberg E, Hsiong S, Kim WJ, Mooney DJ. Dual growth factor delivery and controlled scaffold degradation enhance in vivo bone formation by transplanted bone marrow stromal cells. Bone. 2004; 35(2):562–569. [PubMed: 15268909]

14. Ouyang HW, Goh JCH, Thambyah A, Teoh SH, Lee EH. Knitted Poly-lactide-co-glycolide Scaffold Loaded with Bone Marrow Stromal Cells in Repair and Regeneration of Rabbit Achilles Tendon. Tissue Eng. 2003; 9(3):431–439. [PubMed: 12857411]

15. Madden LR, et al. Proangiogenic scaffolds as functional templates for cardiac tissue engineering. Proc. Natl. Acad. Sci. USA. 2010; 107(34):15211–15216. [PubMed: 20696917]

16. Stachowiak AN, Bershteyn A, Tzatzalos E, Irvine DJ. Bioactive Hydrogels with an Ordered Cellular Structure Combine Interconnected Macroporosity and Robust Mechanical Properties. Adv. Mater. 2005; 17(4):399–403.

17. Golden AP, Tien J. Fabrication of microfluidic hydrogels using molded gelatin as a sacrificial element. Lab Chip. 2007; 7(6):720–725. [PubMed: 17538713]

18. Wang H, Li Y, Zuo Y, Li J, Ma S, Cheng L. Biocompatibility and osteogeneesis of biomimetic nano-hydroxyapatite/polyamide composite scaffolds for bone tissue engineering. Biomaterials. 2007; 28(22):3338–3348. [PubMed: 17481726]

19. Lutolf MP, Weber FE, Schmoekel HG, Schense JC, Kohler T, Müller R, Hubbell JA. Repair of bone defects using synthetic mimetics of collageneous extracellular matrices. Nat Biotechnol. 2003; 21(5):513–518. [PubMed: 12704396]

20. Liu Tsang V, et al. Fabrication of 3D hepatic tissues by additive photopatterning of cellular hydrogels. FASEB J. 2007; 21(3):790–801. [PubMed: 17197384]

21. Prajapati RT, Chavally-Mis B, Herbage D, Eastwood M, Brown RA. Mechanical loading regulates protease production by fibroblasts in three-dimensional collagen substrates. Wound Repair Regen. 2000; 8(3):226–237. [PubMed: 10886813]

22. Bouhadir KH, Lee KY, Alsberg E, Damm KL, Anderson KW, Mooney DJ. Degradation of Partially Oxidized Alginate and Its Potential Application for Tissue Engineering. Biotechnol. Prog. 2001; 17:945–950. [PubMed: 11587588]

23. Gibson, LJ.; Ashby, MF. Cellular Solids. Cambridge: Cambridge University Press; 1997.

24. Diduch DR, Coe MR, Joyner C, Owen ME, Balian G. Two cell lines from bone marrow that differ in terms of collagen synthesis, osteogenic characteristics, and matrix mineralization. J Bone Joint Surg Am. 1993; 75(1):92–105. [PubMed: 8419395]
25. Hsiong SX, Boontheekul T, Huebsch N, Mooney DJ. Cyclic RGD Peptides Enhance 3D Stem Cell Osteogenic Differentiation. Tissue Eng A. 2009; 15(2):263–272.
26. Rowley JA, Madlambayan G, Mooney DJ. Alginate hydrogels as synthetic extracellular matrix materials. Biomaterials. 1999; 20(1):45–53. [PubMed: 9916770]
27. Benoit DS, Schwartz MP, Durney AP, Anseth KS. Small functional groups for controlled differentiation of hydrogel-encapsulated human mesenchymal stem cells. Nat Mater. 2008; 7(10): 816–823. [PubMed: 18724374]
28. Khatiwala CB, Kim PD, Peyton SR, Putnam AJ. ECM compliance regulates osteogenesis by influencing MAPK signaling downstream of RhoA and ROCK. J Bone Miner Res. 2009; 24(5): 886–898. [PubMed: 19113908]
29. DiMilla PA, Stone JA, Quinn JA, Albelda SM, Lauffenburger DA. Maximal migration of human smooth muscle cells on fibronectin and type IV collagen occurs at an intermediate attachment strength. J. Cell Biol. 1993; 122(3):729–737. [PubMed: 8335696]
30. Alsberg E, Anderson KW, Albeiruti A, Rowley JA, Mooney DJ. Engineering growing tissues. Proc. Natl. Acad. Sci. USA. 2002; 99(19):12025–12030. [PubMed: 12218178]
31. Frenette PS, Pinho S, Lucas D, Scheirerman CS. Mesenchymal Stem Cell: Keystone of the Hematopoietic Stem Cell Niche and a Stepping-Stone for Regenerative Medicine. Annu. Rev. Immunol. 2013; 31:285–316. [PubMed: 23298209]
32. Trappmann B, et al. Extracelluar-matrix tethering regulates stem-cell fate. Nat Mater. 2012; 11(7): 642–649. [PubMed: 22635042]
33. Gilbert PM, et al. Substrate Elasticity Regulates Skeletal Muscle Stem Cell Self-Renewal in Culture. Science. 2010; 329:1078–1081. [PubMed: 20647425]
34. Kong HJ, Polte TR, Alsberg E, Mooney DJ. FRET measurements of cell-traction forces and nano-scale clustering of adhesion ligands varied by substrate stiffness. Proc Natl. Acad. Sci. USA. 2005; 102(12):4300–4305. [PubMed: 15767572]
35. Khetan S, Guvendiren M, Legant WR, Cohen DM, Chen CS, Burdick JA. Degradation-mediated cellular traction directs stem cell fate in covalently crosslinked three-dimensional hydrogels. Nat Mater. 2013; 12(5):458–465. [PubMed: 23524375]
36. 40. Yang C, Tibbitt MW, Basta L, Anseth KS. Mechanical memory and dosing influence stem cell fate. Nat Mater. 2014; 13(6):645–652. [PubMed: 24633344]
37. Mammoto T, et al. Mechanochemical control of mesenchymal condensation and embryonic tooth organ formation. Dev Cell. 2011; 21(4):758–769. [PubMed: 21924961]
38. Saha K, et al. Substrate modulus directs neural stem cell behavior. Biophys. J. 2008; 95:4426–4438. [PubMed: 18658232]
39. Sen S, Engler AJ, Discher DE. Matrix strains induced by cells: Computing how far cells can feel. Cell Mol Bioeng. 2009; 2(1):39–48. [PubMed: 20582230]
40. Wang YK, et al. Bone Morphogenic Protein-2 Induced Signaling and Osteogenesis is Regulated by Cell Shape, RhoA/ROCK, and Cytoskeletal Tension. Stem Cells Dev. 2012; 21(7):1176–1186. [PubMed: 21967638]
41. Axelrad TW, Einhorn TA. Bone morphogenetic proteins in orthopaedic surgery. Cytokine & Growth Factor Reviews. 2009; 20:481–4882. [PubMed: 19892584]
42. Platt MO, Wilder CL, Wells A, Griffith LG, Lauffenburger DA. Multipathway kinase signatures of multipotent stromal cells are predictive for osteogenic differentiation: tissue-specific stem cells. Stem Cells. 2009; 27(11):2804–2814. [PubMed: 19750537]
43. Murry CE, Keller G. Differentiation of Embryonic Stem Cells to Clinically Relevant Populations: Lessons from Embryonic Development. Cell. 2008; 132(4):661–680. [PubMed: 18295582]
44. Groen RWY, et al. Reconstructing the human hematopoietic niche in immunodeficient mice: opportunities for studying primary multiple myeloma. Blood. 2012; 120(3):e9–e16. [PubMed: 22653974]

45. Kong HJ, Chan JH, Huebsch N, Weitz D, Mooney DJ. Noninvasive probing of the spatial organization of polymer chains in hydrogels using fluorescence resonance energy transfer (FRET). J. Am. Chem. Soc. 2007; 129(15):4518–4519. [PubMed: 17381090]

46. Kong HJ, Smith MK, Mooney DJ. Designing alginate hydrogels to maintain viability of immobilized cells. Biomaterials. 2003; 24(22):4023–4029. [PubMed: 12834597]

47. Mehta M, Checa S, Lienau J, Hutmacher D, Duda GN. *In vivo* tracking of segmental bone defect healing reveals that callus patterning is related to early mechanical stimuli. Eur. J. Cell. Mater. 2012; 24:358–371.

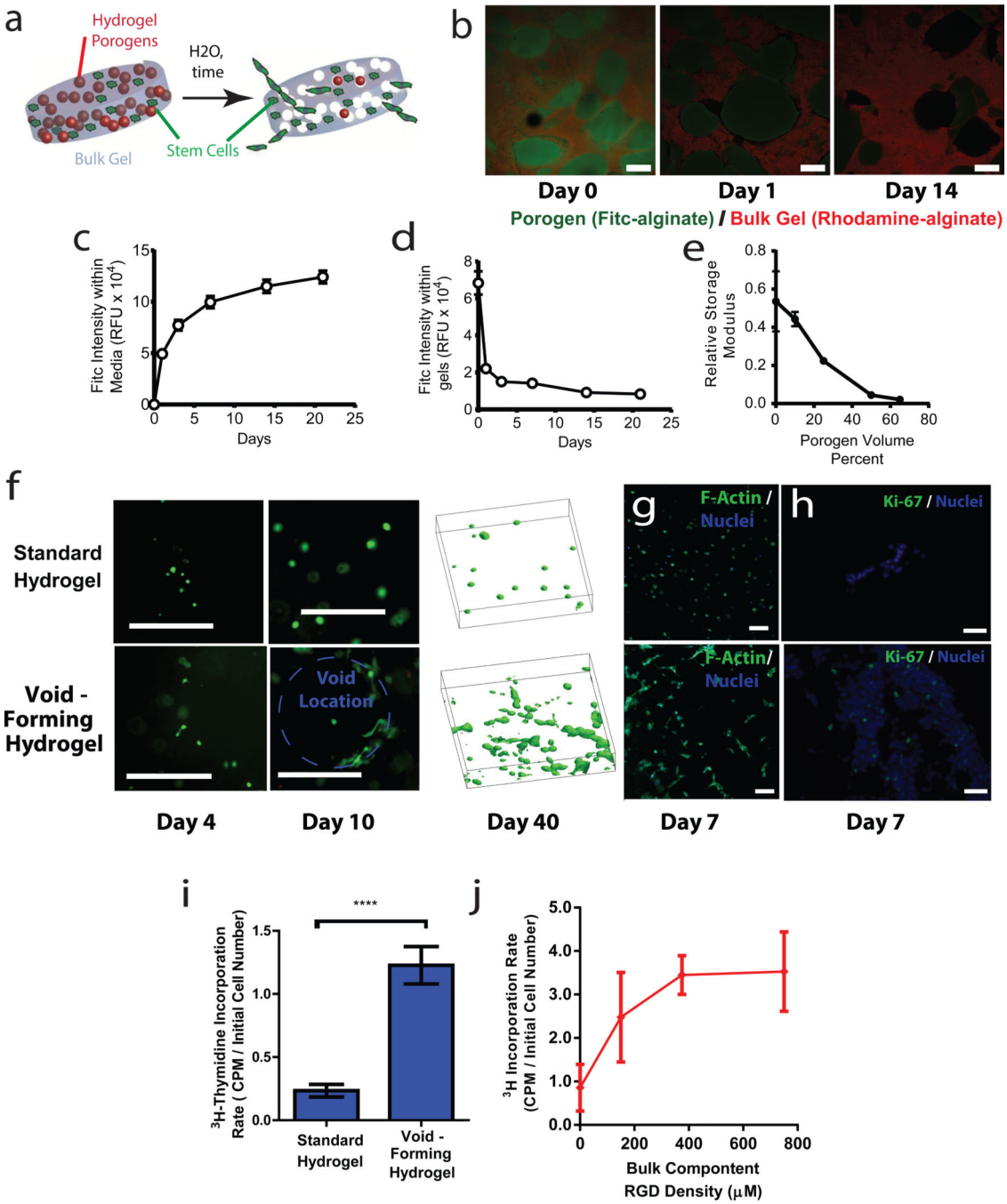

Figure 1. Fabrication and characterization of void-forming hydrogels

(a). Schematic of the strategy to create void-forming hydrogels. Porogens (red) and mesenchymal stem cells (green) are co-encapsulated into a bulk hydrogel (grey). Pores (white) form within the intact bulk hydrogel due to porogen degradation, allowing cell deployment out of the material and into damaged tissues. Note that the rate of cell migration out of the material is expected to be a function of the distance of the cells from the newly formed pores. **(b-e)**. Characterization of void-forming hydrogels. **(b)**. Confocal micrographs of aminofluorescein-labeled porogens (green) within a rhodamine labeled bulk gel (red),

over the time-course of porogen degradation. **(c-d)**. Quantative analysis of the total level of fluorescein, proportional to porogen density, either (c) remaining within gels, or (d) dissolved into media bathing gels. Gels were dissolved into EDTA at set time points to quantify remaining label. **(e)**. Relative shear modulus *G'* of void-forming hydrogels as a function of volume fraction of porogen, 1 week after hydrogel fabrication. Values of *G'* are normalized to the value obtained for a standard hydrogel (no porogen) at day 1. Effects of porogen volume fraction on composite shear modulus were significant ($p < 0.05$, 1-way ANOVA). **(f)**. Morphology of Calcein-AM stained mMSC in standard hydrogels (top) or in void-forming hydrogels (bottom) at day 4 and 10 after encapsulation (dotted blue line denotes void location). To right: 3D projections of Calcein-AM stained cells within either standard gels (top) or void-forming gels (bottom) after 40 days of *in vitro* culture. **(g)**. Representative confocal micrograph of mMSC stained with phalloidin (green, with Hoescht 33342 nuclear counterstain, blue) *in situ* within standard (top) and void forming gel (bottom) at day 7. **(h)** Representative micrographs depicting Ki67 expression (green, with Hoescht 33342 nuclear counterstain, blue) in 10μm cryosections of mMSC in either standard gels (top) or void-forming gels (bottom) at day 7. **(i)** 24 hr ^{3}H-thymidine incorporation by mMSC either in standard gels or void-forming hydrogels 1 week after encapsulation. **(j)** 24 hr ^{3}H-thymidine incorporation by mMSC in void-forming hydrogels wherein the bulk component had a varied level of integrin-binding RGD peptides. RGD density had a significant effect on ^{3}H-incoproration (1-way ANOVA). Error bars are *SD*, $n = 4$ scaffolds. * $p < 0.05$, **** $p < 0.001$, 2-tailed *t*-test. Scale bars: b,c: 1mm (b inset: 200μm); f,h: 100μm; g: 20μm.

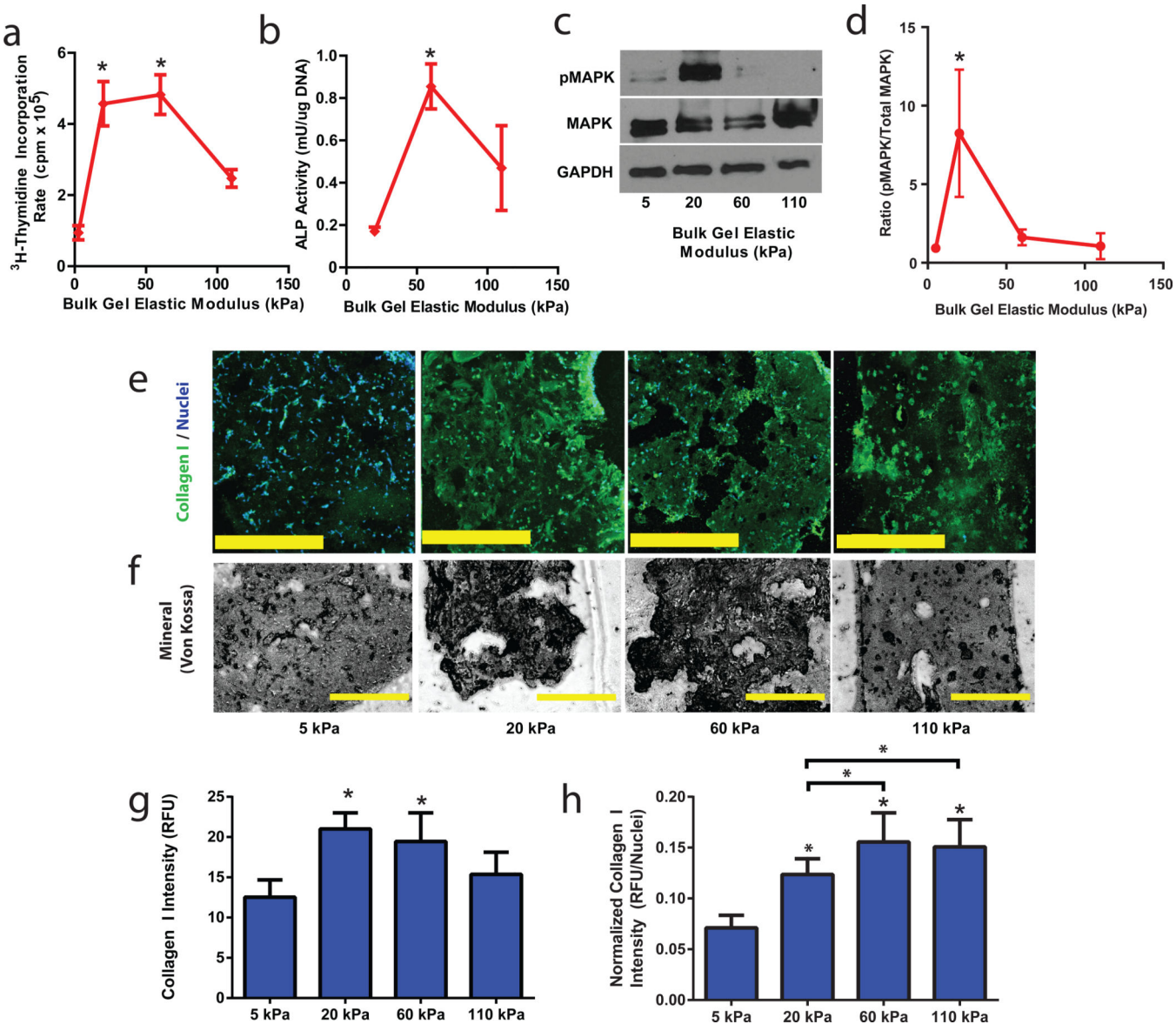

Figure 2. Manipulating Stem Cell Osteogenesis and Proliferation by Controlling the Elasticity of the Bulk Phase of Void-Forming Hydrogels

(a). ^{3}H-thymidine incorporation in last 24 hr by mMSC, after 7 days of culture in void-forming hydrogels, as a function of the elastic modulus of the bulk component. RGD density of gels was constant (375μM). **(b)**. Analysis of Alkaline Phosphatase (ALP; osteogenic biomarker) activity, normalized to the DNA density of mMSC deployed from void forming hydrogels of varying bulk elastic modulus (375μM RGD). Analysis was performed on cells that were released between days 7 and 14 of culture under osteogenic conditions. Bulk gel elasticity had significant effects (one-way ANOVA) on both proliferation and ALP activity. **(c-d)**. Immunoblot analysis of MAPK phosphorylation (anti Phospho-p44/42 MAPK, Thr202/Tyr204) and total MAPK expression for mMSC within void-forming hydrogels as a function of bulk component elasticity, 7 days after gel formation, as depicted by (c) a representative blot and (d) quantitative analysis. GAPDH was used as a loading control for

Western Blots. **(e-h)**. Analysis of (e,f-g,h) Collagen I expression (green; Hoescht 33342 nuclear counterstain, blue) via antibody staining, and analysis of mineralization (f) via Von Kossa staining, of mMSC within void-forming hydrogels of varying bulk component elasticity, after 14 days of culture under osteogenic conditions. **(g-h)**. Quantification of average Collagen I fluorescence signal from 16 cellular regions within the material either (g) without or (h) with normalization to the number of nuclei in each region. Matrix elasticity had a significant effect on Collagen I levels (ANOVA). Error bars: *SD*, $n = 3–5$ biologic replicates. * $p < 0.05$, compared to 5 kPa condition, Holm Bonferroni test, or $p < 0.05$ by 2-way *t*-test with Holm Bonferonni correction for multiple comparisons. Scale bars: d,e: 400μm.

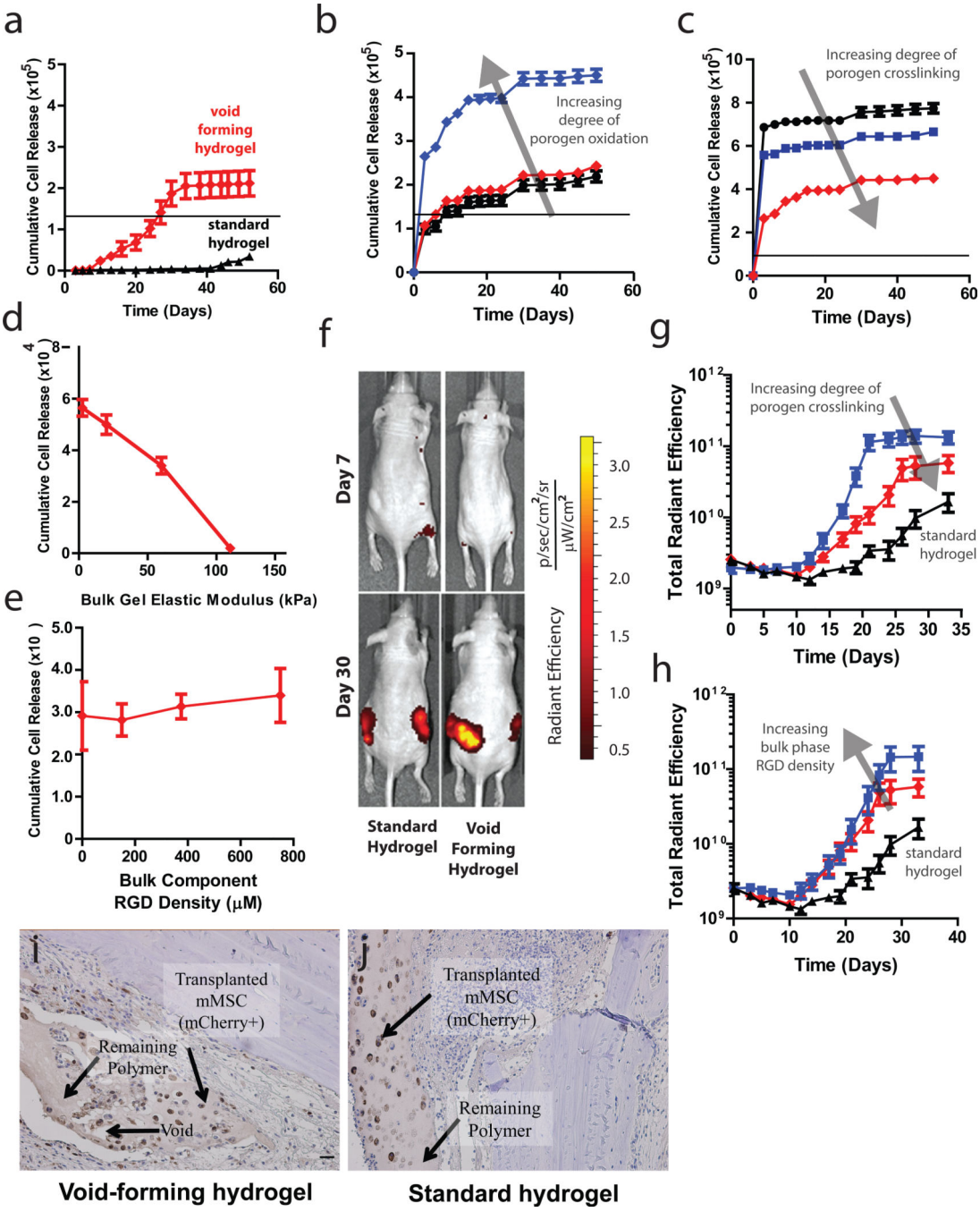

Figure 3. Controlling cell deployment kinetics from void-forming hydrogels *in vitro* and *in vivo*

(a). Kinetic analysis of murine mesenchymal stem cell (mMSC) deployment either from (■) the bulk phase of void-forming hydrogels, or from standard nanoporous hydrogels (▲).The black line denotes the number of cells initially encapsulated into each scaffold. Difference in net cell deployment between the two types of hydrogels was statistically significant ($p < 0.01$, 2-tailed *t*-test) at all time-points. **(b-c)**. Kinetics of mMSC deployment from the bulk phase of void-forming hydrogels as a function of porogen degradation rate, as manipulated by controlling **(b)** the degree of oxidation of polymers used to form porogens (3% (▲), 5%

(♦) or 7.5% (♦)), or **(c)** the concentration of calcium (25mM (●), 50mM (■) or 100mM (♦)) used to crosslink porogens. Net cell deployment was significantly greater from materials with porogens comprised by 7.5% degree of oxidation ($p < 0.001$ at all time points after day 0 by Holm-Bonferonni) compared to deployment from materials with either 3 or 5% degree of oxidation. Each degree of porogen crosslinking yielded a level of net deployment that was statistically unique amongst the different materials tested at all time points after day 0 (Holm-Bonferonni test). **(d)** Analysis of net mMSC deployment at day 7, as a function of the elasticity of bulk component of void-forming gels. Elasticity had a significant effect (1-way ANOVA) on cell deployment. **(e)**. Cumulative cell deployment for mMSC after 1 week of culture in void-forming gels with varying density of RGD peptides. **(f)**. Representative images of Nu/J mice either 7 (top) or 30 (bottom) days after injection of standard (left) or pore-forming hydrogels (right) containing mCherry-expressing mMSC into the subcutaneous tissues of Nu/J mice. **(g)**. Total radiant efficiency (proportional to cell number) from mCherry-mMSC injected within the following hydrogels: void-forming gels with porogens crosslinked with either 100mM (♦) or 50mM (■) Ca^{2+}, or within standard hydrogels (▲). Release of cells from either void-forming hydrogel yielded significantly more release than from a standard hydrogel at all time-points beginning at day 10, and altering porogen fabrication yielded a significant effect on radiant efficiency beginning on day 17 ($p < 0.05$, 2-tailed *t*-test). RGD density was fixed at 187μM in the bulk gel phase. **(h)**. Total radiant efficiency resulting from mCherry-mMSC injected within void-forming hydrogels in which the RGD concentration was either (♦)187μM or (■) 750μM within the bulk phase, or within standard hydrogels (▲). Cell transplantation within either void-forming hydrogel type led to substantially higher total radiant efficiency at all time points after day 12 (187μM RGD) or 19 (750μM RGD), compared to transplantation within standard hydrogels. The difference in total radiant efficiency was affected by the density of RGD presented by the bulk phase beginning on day 24 ($p < 0.05$). **(i-j)** Representative micrographs of tissues in Nude rat cranial defects one week after transplanting mCherry-mMSC with either i) void-forming or j) standard hydrogels. mCherry antigen was probed with DAB chromogen. Error bars are *SEM*, $n = 3–4$ scaffolds (*in vitro* studies) or $n = 4–8$ scaffolds (*in vivo* studies). Scale bar: g,h: 100μm.

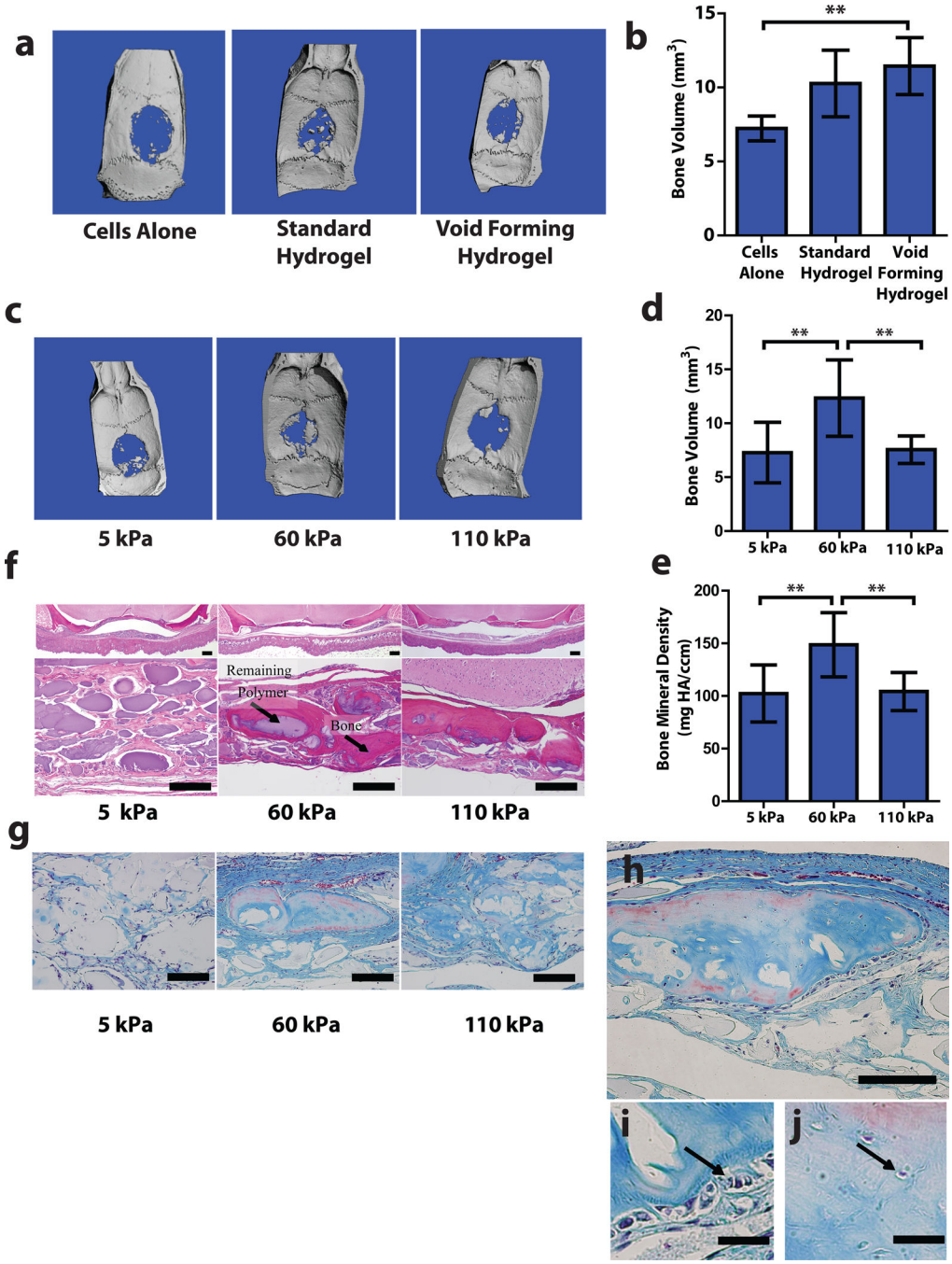

Figure 4. Matrix elasticity regulates mesenchymal stem cell mediated bone regeneration

(a-b). Analysis of bone regeneration in cranial defects due to hMSC transplantation via saline bolus, standard hydrogels or void-forming hydrogels. **(a)**. Representative Micro-Computed Tomographic (μCT) images of regeneration in cranial defects in nude rats 12 weeks after introducing human MSC (hMSC) in saline (Cells Alone), within standard hydrogels or within void-forming hydrogels. **(b)**. Quantitative analysis of the total volume of newly formed bone tissue using μCT. **(c-j)**. Analysis of bone regeneration in cranial defects due to hMSC transplanted in void-forming hydrogels with different bulk-component elastic

moduli. **(c)**. Representative Micro-Computed Tomographic (μCT) images of regeneration in nude rat cranial defects 12 weeks after hMSC delivery in void-forming hydrogels of varying bulk component moduli. **(d-e)**. Quantitative analysis of **(d)** total volume and **(e)** average bone mineral density of regenerated bone. **(f)**. Representative histologic analysis of new bone formation and remaining polymer with Hematoxyln-Eosin staining. **(g)**. Representative Masson's Trichrome staining depicting new bone formation. **(h-j)**. High resolution micrographs depicting trichrome staining of a portion of newly regenerated tissue derived from hMSC transplanted in void forming gels with a bulk modulus of 60 kPa. **(h)** Entire sub-section. **(i-j)**. High resolution images depicting **(i)** osteoblast-like cells at the edge of newly forming tissue, and **(j)** osteocyte-like cells in the central part of newly formed tissues (denoted by black arrows). Error bars: *SD*, $n = 4–5$. ** $p < 0.05$, 2-tailed *t*-test. Scale bars: f-h: 100μm; i-j: 20μm.